MuSt-NeRF: A Multi-Stage NeRF Pipeline to Enhance Novel View Synthesis

Sudarshan Raghavan Iyengar[a], Subash Sharma[b] and Patrick Vandewalle[c]
EAVISE, ESAT-PSI, KU Leuven, Belgium
{*sudarshan.iyengar, patrick.vandewalle*}*@kuleuven.be*

Keywords: Neural Radiance Fields, Novel-View Synthesis, 3D Reconstruction, Depth Priors, View-Dependent Effects.

Abstract: Neural Radiance Fields (NeRFs) have emerged as a powerful technique for novel view synthesis, but accurately capturing both intricate geometry and complex view-dependent effects, especially in challenging real-world scenes, remains a limitation of existing methods. This work presents MuSt-NeRF, a novel multi-stage pipeline designed to enhance the fidelity and robustness of NeRF-based reconstructions. The approach strategically chains complementary NeRF architectures, organized into two stages: a depth-guided stage that establishes a robust geometric foundation, followed by a refinement stage that enhances details and accurately renders view-dependent effects. Crucially, MuSt-NeRF allows flexible stage ordering, enabling either geometry-first or photometry-first reconstruction based on scene characteristics and desired outcomes. Experiments on diverse datasets, including synthetic scenes and complex indoor environments from the ScanNet dataset, demonstrate that MuSt-NeRF consistently outperforms single-stage NeRF and 3D Gaussian Splatting methods, achieving higher scores on established metrics like PSNR, SSIM, and LPIPS, while producing visually superior reconstructions. MuSt-NeRF's flexibility and robust performance make it a promising approach for high-fidelity novel view synthesis in complex, real-world scenes. The code is made available at https://github.com/sudarshan-iyengar/MuSt-NeRF.

1 INTRODUCTION

Reconstructing 3D scenes from a set of images and synthesizing photorealistic novel views is a long-standing challenge in computer vision, with applications in virtual/augmented reality, robotics, and medical imaging (Manni et al., 2021; Lee et al., 2022; Yang et al., 2024).

Neural Radiance Fields (NeRFs) (Mildenhall et al., 2020) have significantly advanced novel view synthesis by representing scenes using a multi-layer perceptron (MLP) that maps 3D locations and viewing directions to color and density, enabling the rendering of photorealistic novel views via differentiable volume rendering.

Despite advancements, NeRFs unfortunately suffer from several drawbacks. Reconstructing accurate geometry from sparse views can lead to artifacts like fogginess and floaters, as traditional NeRF training primarily relies on photometric consistency, which is insufficient to disambiguate between different geometries yielding the same image. Furthermore, representing glossy surfaces and specular reflections accurately is difficult due to the high degree of variation in appearance even with small changes in viewpoint. Existing methods (Wei et al., 2021; Shafiei et al., 2021; Tancik et al., 2022; Barron et al., 2021; Martin-Brualla et al., 2021) often address these challenges individually, creating a need for more holistic solutions.

To address these limitations, we introduce MuSt-NeRF, a multi-stage NeRF pipeline that combines the strengths of complementary NeRF architectures within a flexible, multi-stage framework. By combining a depth-guided geometric foundation stage with a photometric refinement stage, MuSt-NeRF achieves robust performance even with sparse inputs while capturing high-fidelity reflections and handling unbounded scenes. This two-stage approach, with its adaptable geometry-first and photometry-first workflows, allows for optimized performance based on scene characteristics. Our key contributions through this paper are threefold:

1. A novel two-stage NeRF architecture capable of

[a] https://orcid.org/0009-0003-4046-4969
[b] https://orcid.org/0009-0004-1025-460X
[c] https://orcid.org/0000-0002-7106-8024

Iyengar, S. R., Sharma, S. and Vandewalle, P.
MuSt-NeRF: A Multi-Stage NeRF Pipeline to Enhance Novel View Synthesis.
DOI: 10.5220/0013169100003912

In *Proceedings of the 20th International Joint Conference on Computer Vision, Imaging and Computer Graphics Theory and Applications (VISIGRAPP 2025) - Volume 2: VISAPP*, pages 563-573
ISBN: 978-989-758-728-3; ISSN: 2184-4321

handling various scene types, including those with unbounded elements, complex lighting, and a mix of diffuse and specular materials.

2. A flexible pipeline design that supports both geometry-first and photometry-first execution, adapting to varying scene characteristics.

3. A new composite score metric that combines PSNR, SSIM, and LPIPS to provide a perceptually-aligned evaluation of rendering quality. This composite score is used to refine regions of the scene requiring additional photometric or geometric detail.

2 RELATED WORK

2.1 Neural Radiance Fields

Neural Radiance Fields use neural networks to represent a 3D scene as a continuous function. This function, parameterized by a multi-layer perceptron (MLP), takes as input the 3D location $\mathbf{x} = (x, y, z)$ and 2D viewing direction (θ, ϕ) and outputs the radiance $\mathbf{c} = (R, G, B)$ and volume density σ at that point and viewing direction (Mildenhall et al., 2020). The NeRF MLP learns to map 5D input coordinates to the corresponding radiance and volume density values. This can be represented as follows:

$$F_\Theta : (\mathbf{x}, \mathbf{d}) \rightarrow (\mathbf{c}, \sigma) \tag{1}$$

More precisely, positional encoding is applied at the input to the MLP to be able to represent high frequency details more accurately by mapping the inputs to higher degree Fourier features. However, this is omitted from the equation for simplicity.

To render a novel view, NeRF casts a ray $\mathbf{r}(t) = \mathbf{o} + t\mathbf{d}$ (where $\mathbf{o}$ is the camera origin, $\mathbf{d}$ is the ray direction, and t is the distance along the ray) through each pixel into the scene. The color $\mathbf{c}(\mathbf{r})$ and volume density $\sigma(\mathbf{r})$ are then computed at 3D points $\mathbf{r}$ sampled along each ray. These sampled values are integrated within the near and far bounds $[t_n, t_f]$ using the volume rendering equations:

$$T(t) = e^{-\int_{t_n}^{t} \sigma(\mathbf{r}(s))\, ds} \tag{2}$$

$$C(\mathbf{r}) = \int_{t_n}^{t_f} T(t) \cdot \sigma(\mathbf{r}(t)) \cdot \mathbf{c}(\mathbf{r}(t), \mathbf{d})\, dt \tag{3}$$

In practice, the integral is computed in its discretized form using stratified and hierarchical sampling.

This rendering process, while capable of generating high-quality images, presents several limitations. Specifically, NeRF requires a large number of input views for accurate reconstructions, struggles with unbounded scenes, and can exhibit difficulties capturing view-dependent effects, particularly specular reflections.

2.2 Enhancing NeRF - Addressing Its Core Limitations

Several extensions to the original NeRF model have been proposed to address these limitations (Rabby and Zhang, 2023; Gao et al., 2023; Dellaert and Yen-Chen, 2021). A key aspect for improving geometric robustness and enabling training with sparse views is the incorporation of depth information. **Dense Depth Priors NeRF** (Roessle et al., 2022) leverages readily available depth information from Structure-from-Motion (SfM) pipelines, using a depth completion network based on ResNet-18 to generate dense depth and uncertainty maps from sparse point clouds. These maps then guide ray sampling during training and are incorporated into a depth loss term, improving geometric accuracy and reducing reliance on dense input views. MuSt-NeRF employs a similar depth-guided strategy in its initial stage to build a strong geometric foundation, which is the goal of the first stage of MuSt-NeRF.

Handling unbounded scenes is another significant challenge as it implies that content in the scene can lie at arbitrarily far distances (theoretically tending to infinity). The key challenges in applying NeRF-like models to unbounded scenes are finding an effective way to parameterize the 3D space and finding efficient ray sampling strategies. **Mip-NeRF 360** (Barron et al., 2022) addresses these in two ways: Firstly, they introduce a non-linear scene parameterization that maps 3D coordinates onto a bounded sphere, contracting objects that are farther away towards the center, leaving the objects closer and near the center relatively unchanged. Secondly, rather than a single MLP being trained, MipNeRF-360 uses two MLPs: a Proposal MLP which predicts solely volume density, and a NeRF MLP which predicts both volume density and radiance. The Proposal MLP is a smaller and faster MLP that is evaluated multiple times in order to generate a coarse representation of the scene's density distribution and is then used to guide the NeRF MLP's sampling process by informing it of the regions that are likely to contain surfaces. MuSt-NeRF incorporates these strategies within its photometric refinement stage, enabling the representation of unbounded scenes. However, unlike Mip-NeRF 360, MuSt-NeRF also explicitly addresses view-dependent effects, further enhancing realism.

View-dependent effects, particularly specular and glossy reflections, significantly impact the realism of novel views. **Ref-NeRF** (Verbin et al., 2021) tackles this challenge by explicitly modeling reflected radiance using a combination of viewing directions and surface normals. It utilizes an Integrated Directional Encoder (IDE) to capture a distribution of reflection directions and disentangles diffuse and specular components. While Ref-NeRF demonstrates improvements in reflection rendering, it can still be computationally demanding, particularly when combined with techniques for unbounded scenes. MuSt-NeRF integrates the reflection modeling capabilities of Ref-NeRF into its refinement stage. Crucially, by building on the geometrically robust foundation established in the initial stage, MuSt-NeRF mitigates the computational burden and data requirements typically associated with high-fidelity reflection rendering. This combination enables efficient and realistic novel view synthesis even with sparse views and complex lighting.

3 METHOD

Our goal is to synthesize photorealistic novel views of a real-world scene given N input images and their corresponding camera poses, obtained via COLMAP (Schönberger and Frahm, 2016). MuSt-NeRF achieves this through two chained NeRF stages, integrating the strengths of recent NeRF advancements. A depth-guided initial stage builds a strong geometric foundation, which is then refined by a photometric refinement stage. This two-stage approach, with flexible stage ordering (geometry-first or photometry-first), enhances the quality of novel view synthesis.

3.1 Stage 1: Geometric Foundation

This stage focuses on establishing a robust geometric representation of the scene, even from a sparse set of input images. For this, we leverage depth information to guide the NeRF optimization.

First, we obtain camera poses and construct a sparse point cloud using SfM via COLMAP. In the absence of ground truth depth maps, we utilize the sparse point cloud generated by COLMAP and employ a ResNet18-based depth completion network (Roessle et al., 2022) to generate dense depth maps $z(\mathbf{r})$ and corresponding uncertainty maps $s(\mathbf{r})$. The depth maps guide ray sampling during training, concentrating samples in regions with higher object likelihood, as indicated by the depth map and uncertainty estimate. This depth-guided sampling enhances geometric accuracy, especially with sparse view inputs.

The Stage 1 NeRF MLP is trained using a combination of loss functions designed to leverage both photometric information from the RGB images and geometric constraints from the dense depth maps. The total loss function is proposed as a weighted linear combination of the color and depth losses, where λ is a hyperparameter that can be tuned to determine the weight given to the depth loss:

$$\mathcal{L} = \mathcal{L}_{\text{color}}(\mathbf{r}) + \lambda \cdot \mathcal{L}_{\text{depth}}(\mathbf{r}) \tag{4}$$

$$\mathcal{L}_{\text{color}} = \left\| \hat{C}(\mathbf{r}) - C(\mathbf{r}) \right\|_2^2 \tag{5}$$

$$\mathcal{L}_{\text{depth}} = \begin{cases} \log\left(\hat{s}(\mathbf{r})^2\right) + \frac{(\hat{z}(\mathbf{r}) - z(\mathbf{r}))^2}{\hat{s}(\mathbf{r})^2} & \text{if } \alpha \\ 0 & \textit{otherwise} \end{cases} \tag{6}$$

where $\alpha = |\hat{z}(\mathbf{r}) - z(\mathbf{r})| > s(\mathbf{r}) \vee \hat{s}(\mathbf{r}) > s(\mathbf{r})$.

$\mathcal{L}_{\text{color}}$ is a standard loss based on the difference between the rendered and ground truth RGB colors. $\mathcal{L}_{\text{depth}}$ uses the Gaussian Negative Log-Likelihood (GNLL) loss to penalize the model in the following conditions: if the predicted depth $\hat{z}(\mathbf{r})$ differs from the target depth $z(\mathbf{r})$ by more than the target's uncertainty/standard deviation $s(\mathbf{r})$, or if the predicted uncertainty $\hat{s}(\mathbf{r})$ exceeds $s(\mathbf{r})$. In such cases, the GNLL loss is used; otherwise, the loss is zero.

We evaluate the rendered test views using a composite score (range 0-1) based on three metrics, PSNR, SSIM, and LPIPS:

$$\begin{aligned} C = {} & w_{\text{PSNR}} \cdot \left(\frac{\text{PSNR}}{\text{PSNR}_{\max}} \right) \\ & + w_{\text{SSIM}} \cdot \text{SSIM} \\ & + w_{\text{LPIPS}} \cdot (1 - \text{LPIPS}) \end{aligned} \tag{7}$$

Test images with a composite score below a threshold (see Section 4.1), along with their neighboring views, are passed to Stage 2 for refinement. This selection strategy ensures that challenging regions, including those near poorly reconstructed areas, receive additional attention in the refinement stage. The architecture can be seen in Figure 1.

3.2 Stage 2: Photometric Refinement

Building upon the geometric foundation established in Stage 1, this stage refines the scene representation by focusing on high-fidelity rendering of view-dependent effects, particularly specular reflections,

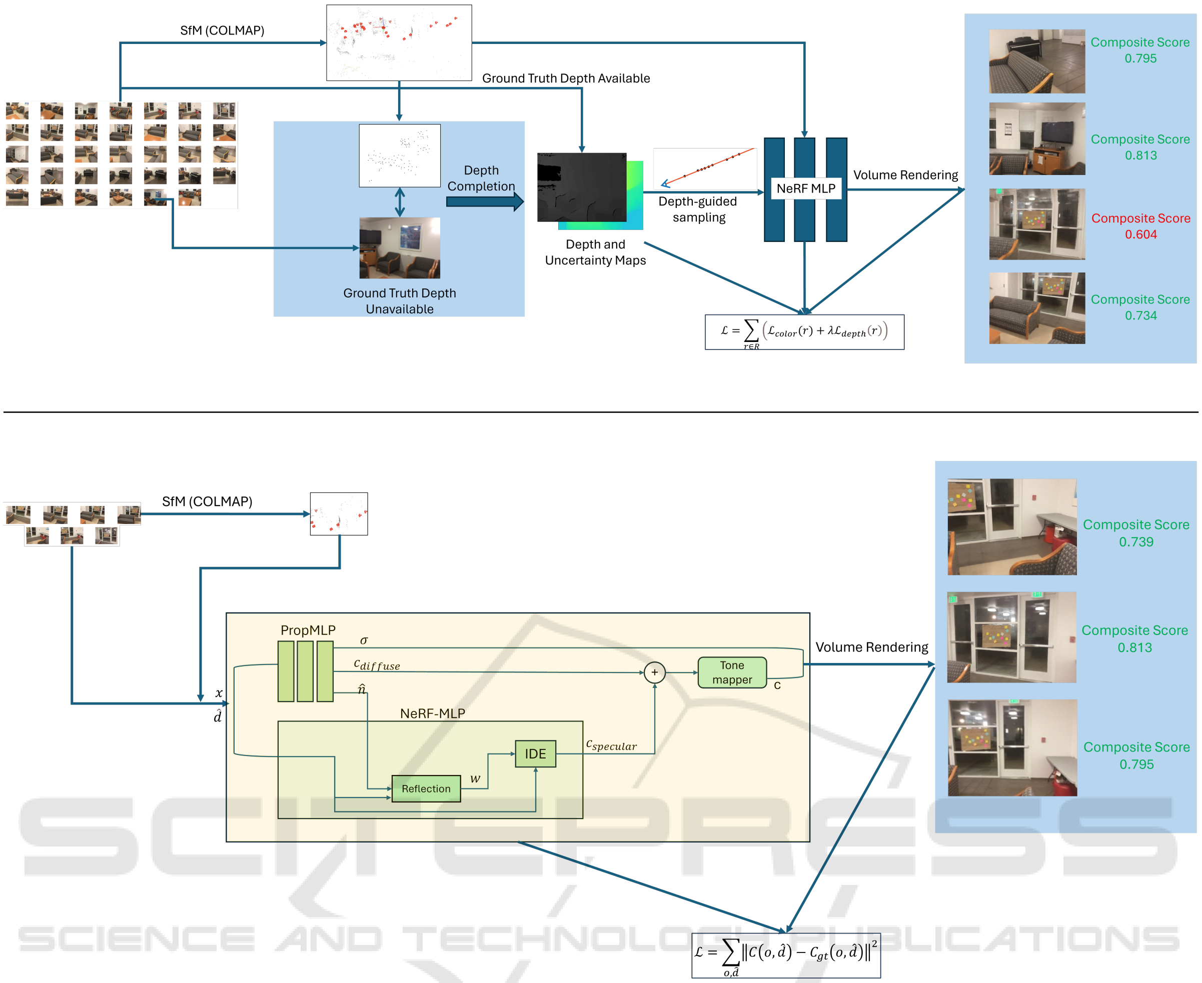

Figure 1: The proposed MuSt-NeRF architecture with Stage 1 on top and Stage 2 below. Stage 1 performs a depth-guided reconstruction using either available ground truth depth maps or depth-completed maps from COLMAP sparse point clouds. Stage 2 performs a photometric-driven reconstruction with a focus on unbounded elements and view-dependent effects.

and handling unbounded scenes. We achieve this by integrating and extending the principles of Mip-NeRF 360 (Barron et al., 2022) and Ref-NeRF (Verbin et al., 2021).

To effectively handle unbounded scenes, we incorporate core elements of Mip-NeRF 360. Specifically, we use a non-linear scene parameterization, which maps scene coordinates onto a unit sphere. This parameterization improves the representation of distant objects by contracting them towards the origin while preserving the relative positions of nearby points. We also employ online distillation by splitting the MLP into a proposal MLP and a NeRF MLP. The proposal MLP's density predictions guide the hierarchical sampling of the NeRF MLP, i.e., more samples are taken in regions where the proposal MLP predicts higher volume density. This concentrates rendering effort on regions likely to contain surfaces, improving efficiency, especially in unbounded scenes.

The NeRF MLP, however, also incorporates key elements to more faithfully represent specular reflections. In addition to the view direction, which traditional NeRF models use, we incorporate predicted surface normals $\hat{\mathbf{n}}$ to the NeRF MLP. The combination of surface normals and view direction enables the explicit modeling of reflected radiance, which is pivotal in obtaining realistic specular reflections. This is achieved by using an Integrated Directional Encoder (Verbin et al., 2021). This encodes a distribution of reflection directions, accounting for surface roughness, allowing the model to effectively represent a wide range of material properties, from diffuse to highly specular. The IDE processes $\hat{\mathbf{n}}, \mathbf{x}$ and $\mathbf{d}$, outputting a specular color $\mathbf{c}_s$. The specular color from the IDE is then combined with the diffuse color from the proposal MLP using a weighted linear combination, which acts as a tone mapper, to get the final color $\hat{\mathbf{c}}$.

The Stage 2 architecture, comprising the proposal and NeRF MLPs described above, is trained using a photometric loss:

$$\mathcal{L}_{\text{color}} = \left\|\hat{C}(\mathbf{r}) - C(\mathbf{r})\right\|_2^2. \tag{8}$$

We also include a regularizer on normals, as done in Ref-NeRF, that penalizes normals oriented away from the camera for samples along the ray that contribute to the final color. This regularizer term enforces volume density to concentrate around surfaces, helping to resolve "foggy" artifacts often seen near reflective surfaces in NeRF outputs.

3.3 Integrating Multi-Stage Outputs

MuSt-NeRF combines the outputs of its two stages to generate the final novel view renderings, including a dynamic walkthrough. Due to coordinate systems varying between the stages, we present a method to align the two, to ensure proper integration of the stages.

Walkthrough Generation. We generate walkthroughs by rendering novel views along smooth camera trajectories created using B-spline interpolation. Key images from the input set define the desired path, and intermediate poses are generated via B-spline interpolation between these key images. Finally, we render novel views from each of these interpolated poses, creating a sequence of images that forms the walkthrough. We empirically observed that a B-spline of degree 1 with 5 to 10 interpolated poses between each pair of key images provides a balance between fine-grained control and efficient computation.

Coordinate System Alignment. After generating a walkthrough with Stage 1 poses, some novel views, particularly those spatially close to regions requiring refinement, may still exhibit artifacts. To address this, we then re-render these views using the trained Stage 2 model.

Since Stage 1 and Stage 2 use different subsets of the original image set as input to COLMAP, their respective coordinate systems are misaligned. Therefore, to obtain an image from an identical pose, we must first align the coordinate systems before rendering.

Our alignment method uses a shared image, present in the input sets of both stages (I_{shared}), as a common reference. This image is typically chosen as the test image from Stage 1 which did not meet the quality threshold from the first stage.

Let $P_{stage1,shared}$ and $P_{stage2,shared}$ be the camera poses of I_{shared} in the Stage 1 and Stage 2 coordinate systems, respectively. The transformation that aligns the Stage 1 coordinate system to the Stage 2 coordinate system can be computed as:

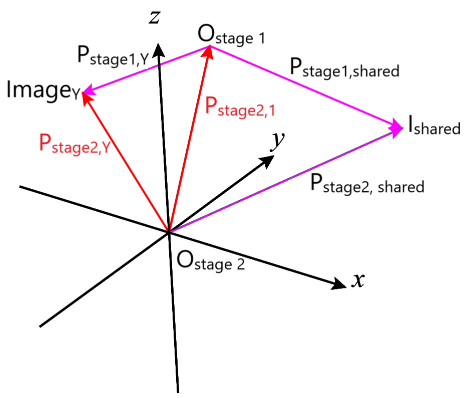

Figure 2: Coordinate System Alignment. The diagram illustrates the relationship between the Stage 1 and Stage 2 coordinate systems.

$$P_{\text{stage2,1}} = P_{\text{stage2,shared}} \cdot (P_{\text{stage1,shared}})^{-1} \tag{9}$$

This transformation is then used to map a novel view pose $P_{stage1,Y}$ from the Stage 1 coordinate system to its Stage 2 equivalent as follows:

$$P_{\text{stage2,Y}} = P_{\text{stage2,1}} \cdot (P_{\text{stage1,Y}}) \tag{10}$$

3.4 Bi-Directionality of MuSt-NeRF

A key feature of MuSt-NeRF is its flexibility in execution order. The pipeline can operate in either a standard geometry-first or a reversed photometry-first mode, adapting to different scene characteristics.

Standard Pipeline (Geometry-First). In this mode, Stage 1 (Geometric Foundation) is executed first, followed by Stage 2 (Photometric Refinement). This approach prioritizes establishing a strong geometric base before refining details and view-dependent effects. It is particularly well-suited for scenes where accurate geometry is paramount, or when working with sparse input views where a robust initial reconstruction is essential. It also improves the rendering of challenging lighting conditions since the geometry is robust.

Reversed Pipeline (Photometry-First). In this mode, Stage 2 (Photometric Refinement) precedes Stage 1 (Geometric Foundation). This approach prioritizes the accurate capture of lighting, reflections, and view-dependent effects. The geometric inaccuracies or inconsistencies stemming from such an architecture can then be rectified through Stage 1. This is beneficial for scenes where fine details and accurate rendering of complex lighting are of primary importance, even at the potential cost of some initial geometric inaccuracies that Stage 1 can often rectify.

The optimal choice between the standard and reversed pipelines depends on the specific scene properties and rendering priorities, as demonstrated in our experiments.

4 EXPERIMENTS

4.1 Implementation Details

Experimental Configurations. To ensure meaningful comparisons, the configurations for each experiment were kept consistent. All experiments were performed on a system equipped with an NVIDIA RTX 2080 Super GPU with 8 GB of VRAM. An overview of the most important configurations can be found in Table 1.

Evaluation Metrics. We evaluate the quality of novel view renderings using three established metrics commonly employed in the NeRF literature: PSNR, SSIM, and LPIPS. In addition to these individual metrics, we also use a composite score, defined in Equation (7), with values for w_{PSNR}, w_{SSIM}, w_{LPIPS}, and $PSNR_{max}$ set to 0.20, 0.35, 0.45, and 35 dB, respectively. These weights prioritize perceptually aligned metrics (LPIPS and SSIM) over purely pixel-based comparisons (PSNR), reflecting human visual perception of scene similarity. A threshold on this composite score is used to determine if an image from Stage 1 needs to be refined in Stage 2. This threshold was experimentally set to 0.7, based on qualitative assessment of rendered image quality: images with composite scores below 0.7 exhibited noticeable artifacts and were deemed unsatisfactory.

4.2 Results and Analysis

We evaluate MuSt-NeRF on increasingly complex scenes. Preliminary experiments validate the effectiveness of our Stage 2 photometric refinement, while also highlighting the need for a multi-stage approach. Subsequent experiments on challenging ScanNet scenes then demonstrate the performance of the full MuSt-NeRF pipeline, comparing the standard and reversed configurations.

Table 1: Overview of the fundamental configurations used in MuSt-NeRF experiments.

Parameter	Stage 1	Stage 2
Number of Epochs	200k	400k
Batch size	1024	512
MLP layers	8	Prop, NeRF: 4,8
Neurons per layer	256	Prop, NeRF: 256,512
Image resolution (px)	624x468	624x468

4.2.1 Preliminary Experiments

These experiments isolate and evaluate the Stage 2 architecture, demonstrating its ability to handle both unbounded scenes and specular reflections, while also motivating the need for a multi-stage approach. We use the following datasets:

Mip-NeRF 360 (Materials, Vasedeck): The *Materials* scene features round balls of diverse material properties under controlled lighting, enabling assessment of specular reflection capture. The *Vasedeck* scene is a real-world capture of flowers, primarily exhibiting diffuse reflections, allowing us to evaluate performance on real-world data with simpler lighting.

Custom Dataset (Plant on Table, Room): The *Plant on Table* scene combines diffuse and specular reflections with unbounded elements (background visible through glass). The *Room* scene (real-world, smartphone, inside-out) provides a more challenging test with complex geometry and lighting.

Table 2 presents the quantitative results of these experiments, comparing MuSt-NeRF Stage 2 with Mip-NeRF 360.

The preliminary experiments evaluate MuSt-NeRF Stage 2 on increasingly complex outside-in scenes. Beginning with the synthetic *Materials* scene, we observe that MuSt-NeRF Stage 2 accurately renders specular highlights, achieving an average composite score of over 0.9 (Table 2, Figure 3). Through the *Vasedeck* scene, we see that MuSt-NeRF Stage 2 is able to handle real-world scenes, performing comparably to the Mip-NeRF 360 implementation. The subsequent experiment on the *Plant on Table* scene further confirms MuSt-NeRF Stage 2's ability to handle unbounded elements as well as specular and diffuse reflections. It is important to note here that each of the test images scored higher than the threshold of 0.7 in these three experiments.

Based on these results, we evaluate Stage 2 on the Room scene, which is an inside-out scenario. We observe that here too, MuSt-NeRF Stage 2 performs better than Mip-NeRF 360 on average (Table 2), and is able to capture reflections effectively (Figure 4). However, we also observe some geometric inaccuracies, especially in regions with high depth variation and with limited overlapping viewpoints between images. It is in these regions that the composite score of MuSt-NeRF is lower than the threshold (Table 3). These limitations, arising from Stage 2's purely photometric nature, emphasize the need for a geometri-

Table 2: Quantitative Results of the Preliminary Experiments - Performance Comparison between Mip-NeRF 360 and MuSt-NeRF Stage 2.

	Mip-NeRF 360				MuSt-NeRF Stage 2			
Scene	**SSIM ↑**	**PSNR ↑**	**LPIPS ↓**	**Composite Score ↑**	**SSIM ↑**	**PSNR ↑**	**LPIPS ↓**	**Composite Score ↑**
Materials	0.897	26.905	0.093	0.876	0.961	27.301	0.029	**0.929**
Vasedeck	0.793	24.592	0.189	**0.783**	0.723	24.409	0.205	0.750
Plant	0.742	25.108	0.255	0.738	0.757	24.905	0.249	**0.746**
Room	0.738	25.674	0.234	0.750	0.830	26.102	0.210	**0.795**

(a) Ground Truth Synthesized

(b) Ground Truth Synthesized

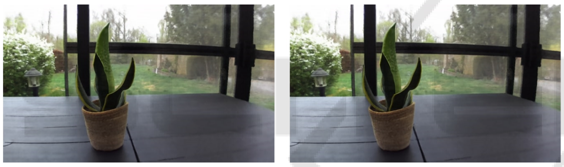

(c) Ground Truth Synthesized

Figure 3: Preliminary Experiments: a- Materials, b- Vasedeck, c- Plant. Zoom in for a clearer view.

cally robust foundation, i.e., Stage 1 of MuSt-NeRF, and the subsequent evaluation of our full pipeline.

4.2.2 ScanNet Experiments

Building upon the insights from our preliminary experiments, we now evaluate the full MuSt-NeRF pipeline (Stages 1 and 2) on five diverse scenes from the ScanNet dataset (Dai et al., 2017). The provided RGB-D images of real-world indoor environments enable us to assess performance on complex, realistic data while leveraging ground truth depth. Furthermore, we investigate the necessity of ground truth depth by comparing performance using both ground truth and depth-completed maps (derived from sparse point clouds, as shown in Stage 1 of Figure 1).

The selected scenes exhibit varied characteristics, including challenging lighting conditions, complex geometry, and varying object density: Scene 708 (dimly lit), Scene 710 (small, densely cluttered), Scene 738 (hotel room with unbounded el-

Table 3: Quantitative Evaluation Results of the Inside-Out Room scene.

IMAGE	SSIM ↑	PSNR ↑	LPIPS ↓	Composite Score ↑
1	0.781	21.012	0.278	0.718
2	0.882	23.372	0.111	0.843
3	0.866	26.441	0.165	0.830
4	0.927	27.690	0.089	0.893
5	0.807	26.320	0.247	0.772
6	0.861	26.390	0.135	0.842
7	0.930	30.609	0.071	0.918
8	0.857	24.451	0.186	0.806
9	0.924	30.509	0.081	0.911
10	0.878	27.618	0.159	0.844
11	0.870	27.682	0.146	0.847
12	**0.720**	**24.792**	**0.432**	**0.650**
13	0.854	28.526	0.181	0.830
14	0.757	18.791	0.260	0.705
15	0.784	27.045	0.286	0.750
16	**0.585**	**26.389**	**0.536**	**0.564**
Average	0.830	26.102	0.210	0.795

(a) Ground Truth Synthesized

(b) Ground Truth Synthesized

Figure 4: Preliminary Experiments - Room Scene: a- Rendered image with a high composite score, b- Rendered image scoring below the threshold. Zoom in for a clearer view.

Table 4: Quantitative Results of the ScanNet Experiments - Performance Comparison among Mip-NeRF 360, 3D Gaussian Splatting, and MuSt-NeRF.

	Mip-NeRF 360				3D Gaussian Splatting				MuSt-NeRF			
Scene	**SSIM ↑**	**PSNR ↑**	**LPIPS ↓**	**Composite Score ↑**	**SSIM ↑**	**PSNR ↑**	**LPIPS ↓**	**Composite Score ↑**	**SSIM ↑**	**PSNR ↑**	**LPIPS ↓**	**Composite Score ↑**
Scene 708	0.752	25.101	0.274	0.733	0.746	21.022	0.315	0.689	0.846	27.208	0.180	**0.821**
Scene 710	0.750	22.704	0.214	0.746	0.727	18.700	0.436	0.615	0.788	24.336	0.185	**0.782**
Scene 758	0.845	26.403	0.119	0.843	0.816	23.373	0.364	0.705	0.857	26.698	0.128	**0.845**
Scene 781	0.803	25.487	0.252	0.763	0.706	18.406	0.311	0.662	0.826	26.872	0.159	**0.821**

Table 5: Quantitative Results on ScanNet Scenes - Comparison of the Standard and Reversed Pipelines of MuSt-NeRF. The optimal choice for each scene is highlighted in bold.

Scene	Configuration	SSIM ↑	PSNR ↑	LPIPS ↓	Composite Score ↑
Scene 708	**Standard**	0.846	27.208	0.180	**0.821**
	Reversed	0.796	25.617	0.238	0.768
Scene 710	Standard	0.783	20.497	0.207	0.748
	Reversed	0.788	24.336	0.185	**0.782**
Scene 738	**Standard No refinement**	0.706	19.427	0.192	**0.722**
	Reversed	-	-	-	-
Scene 758	Standard	0.808	21.962	0.160	0.786
	Reversed	0.857	26.698	0.128	**0.845**
Scene 781	Standard	0.776	22.829	0.175	0.773
	Reversed	0.826	26.872	0.159	**0.821**

ements), Scene 758 (medium-sized room with simple lighting), and Scene 781 (large room with complex lighting and specular reflections). We compare the performance of both the standard (geometry-first) and reversed (photometry-first) MuSt-NeRF configurations with Mip-NeRF 360 and 3D Gaussian Splatting (Kerbl et al., 2023). The results of the ScanNet experiments are shown in Table 4, Table 5 and Figure 6. The results highlight four main findings of the MuSt-NeRF architecture.

Benefits of Multi-Stage Refinement. The most compelling finding from our ScanNet experiments is the consistent and significant improvement achieved through multi-stage refinement. In both the standard and reversed pipelines, the refinement stage effectively leverages the strengths of one stage to mitigate the weaknesses of the other, leading to clearly enhanced performance, as seen through Table 4 and Table 5.

In the standard pipeline, we see that the NeRF model is not able to capture details of the piano (Scene 710), books (Scene 758) or model reflections from multiple light sources (Scene 781) accurately. The refinement stage of the standard pipeline excels at modeling specifically these, leading to an improvement in the composite score as well as in visual comparisons (Figure 6).

Similarly, in the reverse pipeline, we see that the photometric reconstruction incorrectly infers the geometry of the open blinds (Scene 710). The depth-guided training in the refinement stage corrects this error, resulting in a more accurate and visually convincing representation. Again, the composite scores and visual comparisons highlight the enhanced performance achieved through multi-stage refinement.

When comparing Mip-NeRF 360 and 3D Gaussian Splatting to MuSt-NeRF, we see that MuSt-NeRF consistently outperforms the two 360 across all four scenes, with the most prominent difference being in low-lighting scenes (Scene 708) and large scenes (Scene 781) where the benefits of the geometry-guided stage is most strongly observed. It is essential to note that each test image for each of the experiments exceeded the composite score threshold after the entire MuSt-NeRF pipeline, a benchmark that Mip-NeRF 360 and, especially, 3D Gaussian Splatting failed to meet consistently. The underperformance of 3D Gaussian Splatting can likely be attributed to the limited number of input images and the resulting sparsity of the point clouds generated for these scenes. This sparsity leads to insufficient overlap between Gaussians, hindering their ability to blend smoothly and produce high-quality reconstructions.

Influence of Lighting and Scene Characteristics. Lighting conditions and scene complexity significantly impact the relative performance of the standard and reversed pipelines. The standard (geometry-first) pipeline demonstrates greater robustness in challenging lighting, particularly in the dimly lit Scene 708 (Table 5). The reversed (photometry-first) pipeline excels in scenes with complex lighting and specular reflections, such as Scene 781 (Table 5). Scenes with simpler lighting and geometry, like Scene 758, show very similar performance with both configurations. These observations demonstrate MuSt-NeRF's adaptability: the choice of pipeline can be tailored to the scene's specific characteristics and rendering priorities. The depth guidance in Stage 1 of the standard pipeline provides a strong geometric prior, which is beneficial in dimly lit scenes, whereas prioritizing photometric refinement by performing the reversed pipeline allows for more accurate capture of complex lighting.

Influence of Image Quality. We also analyze how variations in image quality affect MuSt-NeRF. Scene 738 of the ScanNet dataset contains several blurry images (see Figure 5). The lack of sharpness hampers COLMAP's ability to extract features and estimate poses accurately, leading to incomplete or erroneous pose information. In Scene 738, COLMAP failed to find sufficient poses for images in regions rendered poorly during Stage 1, preventing subsequent Stage 2 refinement. In the reversed pipeline for the same scene, COLMAP was only able to extract 4 poses from a set of 67 images, which is inadequate for reliable training of the Stage 2 architecture (Table 5).

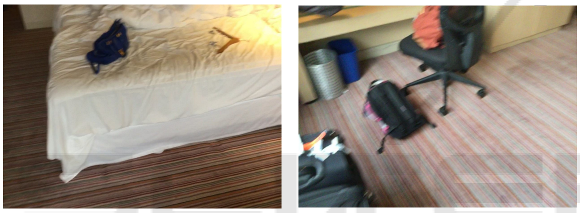

(a) Example blurry images from the dataset.

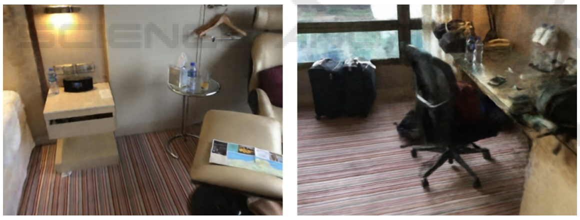

(b) Rendered image with the highest and lowest composite scores respectively.

Figure 5: Scene 738 - Blurry images from the dataset, best, and worst-scoring synthesized images.

There is an additional issue that poor image quality presents. Even if COLMAP successfully extracts poses from these images, the NeRF model's learning process is negatively impacted. The model will learn the inherent blurriness present in the training images, leading to suboptimal novel view synthesis. The rendered outputs will inherit this blurriness, even in regions where sharper details could potentially be recovered with higher-quality input images. This highlights the importance of high-quality input images for optimal performance and the data-driven nature of NeRF-based approaches.

Sufficiency of Depth-Completed Maps. To validate the influence of depth map quality on MuSt-NeRF, we conducted supplementary experiments comparing performance with ground truth depth maps against performance with depth-completed maps. Specifically, we evaluated ScanNet scenes 738 and 758 using the standard (geometry-first) MuSt-NeRF configuration with ground truth depth obtained directly from the ScanNet dataset. These results complement our primary ScanNet experiments (Tables 4 and 5), which utilized depth-completed maps derived from sparse point clouds. The comparative findings are presented below.

Table 6: Comparison of Composite Scores using Ground Truth and Depth-Completed Maps.

Scene	True Depth Map ↑	Depth-Completed Map ↑
738	**0.724**	0.722
758	0.780	**0.786**

These experiments reveal comparable performance between ground truth depth maps and depth-completed maps in Stage 1 of MuSt-NeRF (Table 6). This suggests that the depth completion network produces depth estimates that are sufficiently precise to guide the geometric reconstruction effectively. Consequently, it also points to the practical versatility of MuSt-NeRF, as it is not dependent on the availability of RGB-D data for optimal performance.

5 CONCLUSION

In this work, we presented MuSt-NeRF, a novel two-stage NeRF pipeline that enhances novel view synthesis by addressing the challenges of unbounded scenes, complex lighting, and view-dependent effects, particularly specular reflections. MuSt-NeRF combines a depth-guided geometric foundation stage with a photometric refinement stage, integrating and extending principles from Mip-NeRF 360 and Ref-NeRF. Our approach provides flexibility by supporting both geometry-first and photometry-first execution modes, allowing users to adapt the pipeline to different scene characteristics and rendering priorities.

Our experiments on a variety of scenes, including synthetic data, real-world captures, and challenging indoor environments from the ScanNet dataset, demonstrated the effectiveness of MuSt-NeRF. We showed that our two-stage approach consistently outperforms the single-stage Mip-NeRF 360 baseline. The preliminary experiments validated the photometric refinement stage's capabilities in capturing complex lighting, reflections and handling unbounded elements, showcasing the strengths of our combined

(a) Scene 708.

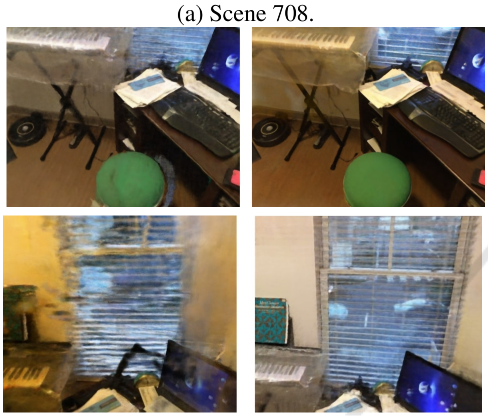

(b) Scene 710.

(c) Scene 758.

(d) Scene 781.

Figure 6: ScanNet Experiments: Top pair per scene shows the standard pipeline before and after refinement, while the bottom pair shows the reverse pipeline.

Mip-NeRF 360 and Ref-NeRF architecture, while the ScanNet experiments highlighted the benefits of our full pipeline, including the importance of the depth-guided stage for geometric robustness, the flexibility of both the standard and reverse pipeline configurations, and MuSt-NeRF's robustness to variations in lighting conditions. Furthermore, the results indicated that the choice between the standard and reversed pipelines depends on scene properties: the standard pipeline excels in low-light scenarios and in scens with limited views, while the reversed pipeline is better suited for scenes with complex reflections and fine details where photometric accuracy is paramount. Potential future work includes evaluating MuSt-NeRF on a wider variety of scene types, such as outdoor environments or scenes with transparent objects and benchmarking against newer NeRF and Gaussian Splatting variants.

REFERENCES

Barron, J. T., Mildenhall, B., Tancik, M., Hedman, P., Martin-Brualla, R., and Srinivasan, P. P. (2021). Mip-NeRF: A Multiscale Representation for Anti-Aliasing Neural Radiance Fields. arXiv:2103.13415.

Barron, J. T., Mildenhall, B., Verbin, D., Srinivasan, P. P., and Hedman, P. (2022). Mip-nerf 360: Unbounded anti-aliased neural radiance fields.

Dai, A., Chang, A. X., Savva, M., Halber, M., Funkhouser, T., and Nießner, M. (2017). Scannet: Richly-annotated 3d reconstructions of indoor scenes.

Dellaert, F. and Yen-Chen, L. (2021). Neural volume rendering: Nerf and beyond.

Gao, K., Gao, Y., He, H., Lu, D., Xu, L., and Li, J. (2023). Nerf: Neural radiance field in 3d vision, a comprehensive review.

Kerbl, B., Kopanas, G., Leimkühler, T., and Drettakis, G. (2023). 3d gaussian splatting for real-time radiance field rendering. *ACM Transactions on Graphics*, 42(4).

Lee, S., Chen, L., Wang, J., Liniger, A., Kumar, S., and Yu, F. (2022). Uncertainty Guided Policy for Active Robotic 3D Reconstruction Using Neural Radiance Fields. *IEEE Robotics and Automation Letters*, 7(4):12070–12077. Conference Name: IEEE Robotics and Automation Letters.

Manni, A., Oriti, D., Sanna, A., De Pace, F., and Manuri, F. (2021). Snap2cad: 3D indoor environment reconstruction for AR/VR applications using a smartphone device. *Computers & Graphics*, 100:116–124.

Martin-Brualla, R., Radwan, N., Sajjadi, M. S. M., Barron, J. T., Dosovitskiy, A., and Duckworth, D. (2021). Nerf in the wild: Neural radiance fields for unconstrained photo collections.

Mildenhall, B., Srinivasan, P. P., Tancik, M., Barron, J. T., Ramamoorthi, R., and Ng, R. (2020). NeRF: Representing Scenes as Neural Radiance Fields for View Synthesis. arXiv:2003.08934 [cs].

Rabby, A. S. A. and Zhang, C. (2023). Beyondpixels: A comprehensive review of the evolution of neural radiance fields. *arXiv e-prints*, pages arXiv–2306.

Roessle, B., Barron, J. T., Mildenhall, B., Srinivasan, P. P., and Nießner, M. (2022). Dense depth priors for neural radiance fields from sparse input views.

Schönberger, J. L. and Frahm, J.-M. (2016). Structure-from-motion revisited. In *Conference on Computer Vision and Pattern Recognition (CVPR)*.

Shafiei, M., Bi, S., Li, Z., Liaudanskas, A., Ortiz-Cayon, R., and Ramamoorthi, R. (2021). Learning Neural Transmittance for Efficient Rendering of Reflectance Fields. arXiv:2110.13272.

Tancik, M., Casser, V., Yan, X., Pradhan, S., Mildenhall, B., Srinivasan, P. P., Barron, J. T., and Kretzschmar, H. (2022). Block-NeRF: Scalable Large Scene Neural View Synthesis. arXiv:2202.05263 version: 1.

Verbin, D., Hedman, P., Mildenhall, B., Zickler, T., Barron, J. T., and Srinivasan, P. P. (2021). Ref-nerf: Structured view-dependent appearance for neural radiance fields.

Wei, Y., Liu, S., Rao, Y., Zhao, W., Lu, J., and Zhou, J. (2021). NerfingMVS: Guided Optimization of Neural Radiance Fields for Indoor Multi-view Stereo. arXiv:2109.01129.

Yang, Z., Dai, J., and Pan, J. (2024). 3D reconstruction from endoscopy images: A survey. *Computers in Biology and Medicine*, 175:108546.